photonics

MDPI

Article

Dynamic Light Scattering by Foamed Polymers during Preparation of Scaffold Prototypes: Events Statistics Analysis versus Evaluation of Correlation Time in Data Interpretation

Dmitry Zimnyakov [1,2,*], Marina Alonova [1], Ekaterina Ushakova [1], Olga Ushakova [1], Anna Isaeva [1] and Elena Isaeva [1]

[1] Physics Department, Yury Gagarin State Technical University of Saratov, 77 Polytechnicheskaya st., 410054 Saratov, Russia; alonova_marina@mail.ru (M.A.); katushakova96@yandex.ru (E.U.); s_sov@rambler.ru (O.U.); isanna.1987@mail.ru (A.I.); 27isaevaea@mail.ru (E.I.)

[2] Precision Mechanics and Control Institute of Russian Academy of Sciences, 24 Rabochaya st., 410024 Saratov, Russia

* Correspondence: zimnykov@mail.ru; Tel.: +7-845-299-8624

Abstract: Polylactide foaming as the key stage in laboratory preparation of highly porous biocompatible matrices used as scaffold prototypes was monitored based the effect of dynamic light scattering in expanding polylactide foams. Intensity fluctuations of scattered laser radiation in the course of foam expansion were analyzed using ensemble-averaged estimates of the speckle lifetime within a running window in the time domain. It was found that, in contrast to the commonly used correlation time of intensity fluctuations, the values of the average speckle lifetime are invariant with respect to the type of dynamics of phase fluctuations of partial components in scattered radiation. This makes it possible to relate this parameter to microscopic mobility of interphase boundaries in the foam in the absence of *a priori* information on the law of motion relating these boundaries at the microscopic level. The proposed approach in combination with the developed phenomenological model describing the relationship between the average speckle lifetime and the current values of the foam volume, as well as its first-time derivative made it possible to interpret the features of foam structure formation.

Keywords: dynamic light scattering; scaffold synthesis; polylactide foam; average speckle lifetime; correlation time

Citation: Zimnyakov, D.; Alonova, M.; Ushakova, E.; Ushakova, O.; Isaeva, A.; Isaeva, E. Dynamic Light Scattering by Foamed Polymers during Preparation of Scaffold Prototypes: Events Statistics Analysis versus Evaluation of Correlation Time in Data Interpretation. *Photonics* **2021**, *8*, 549. https://doi.org/10.3390/photonics8120549

Received: 5 November 2021
Accepted: 1 December 2021
Published: 3 December 2021

1. Introduction

Development and implementation of technologies for the synthesis of biocompatible functional materials is a sounding trend in such areas of modern life sciences as biomedical diagnostics, therapy, surgery, and tissue engineering. Among a wide variety of these materials with various functional purposes, we can single out a class of highly porous bioresorbable matrices. Such matrices synthesized using biocompatible and biodegradable polymers are usually considered as a material platform for creation of scaffolds used in tissue engineering and regenerative medicine [1–3]. Currently, there are several technologies for creating highly porous scaffold prototypes with the required morphological and functional characteristics (i.e., an average pore size and variance of pore size distribution, a degree of pore interconnectivity, volume-averaged porosity, biodegradation rate, etc.).

One of these technologies involves the procedure associated with foaming the raw biocompatible polymer, preliminary plasticized in the atmosphere of a supercritical plasticizing/foaming agent. A significant contribution to the development of this approach and its implementation has been made in the past two decades by several research teams (see, e.g., [4–10]). Formation and expansion of the polymer foam in the "polymer-plasticizing agent" system occurs due to the changes in external parameters (pressure and temperature) according to the given scenario, which has a crucial influence on the structural properties of the formed porous matrix. Note that the use of pressure as the governing parameter in

this procedure is usually more preferable than using the temperature due to significant thermal inertia of the foamed system with the environment.

Evolution of the polymer foam because of depressurization of the "plasticized polymer-plasticizing/foaming agent" system is a complex nonstationary process that depends on a variety of external and internal parameters and includes three essential stages. These stages are formation of an ensemble of cell embryos due to nucleation, intensive cell growth and formation of the foam structure during its expansion, and stabilization of the foam structure. From a physical standpoint, all these changes occur due to constant displacement of the system in time in relation to its current quasi-equilibrium state. The most significant changes in the structure of the evolving foam, caused by intense motion of interphase boundaries at the microscopic level, occur at the second stage and radically affect the structure of the synthesized highly porous matrix. A remote monitoring of these local motions of interphase boundaries in the working area of a high-pressure reactor using traditional approaches (for example, acoustic, X-ray, electron microscopic, etc.) is not feasible due to a number of fundamental limitations characteristic of these approaches. These limitations include rapid dynamics of the structural changes in the probed samples and a need for special preparation of specimens, geometric constraints, sensitivity to environment, etc. Consequently, a relationship between the parameters of the foaming process (initial pressure and temperature, the depressurization rate) and the structural characteristics of the synthesized highly porous matrices is established in the *a posteriori* mode upon completion of the stabilization stage [6,7,9–11]. In turn, the choice of the foaming mode that provides the desired parameters of the scaffold prototype is usually made using a trivial trial-and-error approach or, at best, as a result of a multivariate experiment with a subsequent regression analysis of the obtained data.

At the same time, monitoring the local dynamics of interphase boundaries in the expanding polymer foams seems useful not only for further development of the technologies used for the synthesis of highly porous functional materials applied in biomedicine. In general, it can also contribute to a deeper understanding of the fundamental features in the behavior of essentially nonstationary two-phase systems at the microscopic level. Among a wide variety of remote sensing techniques, the methods based on the dynamic scattering of laser light (DLS) seem to be preferable for characterizing the local dynamics of interphase boundaries in expanding foams. In addition to high sensitivity of scattered radiation to the local dynamics of scattering centers, these methods are characterized by the presence of a "built-in length standard", such as the wavelength of probe light. This makes it possible to measure the parameters of the scatter mobility (the velocity or diffusion coefficient) in absolute units (e.g., $\mu m/s$, $\mu m^2/s$). Accordingly, such generalized parameter of intensity fluctuations of scattered radiation as the correlation time can be assigned to the mobility of scattering centers in the presence of this built-in length standard. However, such assignment will be correct only in the case of exact *a priori* definition of the motion law of scattering centers on the scale of the order of the wavelength used. This definition meets no problems in the case of stationary scattering systems with well-established behavior (for instance, the Brownian ensembles or regular flows of particles). At the same time, the problem relating the type of local dynamics of the scattering sites in such essentially nonstationary systems as rapidly evolving foams is not completely clear; the preliminary assumptions that the local dynamics of scatterers (interphase boundaries) in these systems can be described in terms of only their diffusion-like or drift-like motions cannot be correctly substantiated. Moreover, the type of local dynamics of the cell walls (the basic scattering units) in expanding foams can significantly change with expanding of the cells.

That is why the choice of an adequate approach to analyzing the data on dynamic light scattering, which makes it possible to bypass these traps, seems to be significant. Accordingly, the goal of this work is to substantiate and verify the method for analyzing the data on the dynamic scattering of laser radiation in evolving polymer foams, which does not require preliminary assumptions about the type of dynamics of the scattering centers in the probed medium. Pilot studies of DLS probing of expanding polymer foams using the

stacked speckle history (SSH) technique were carried out in [12], and the average speckle lifetime estimated using SSH maps was considered as a possible informative parameter for characterizing the microscopic dynamics in the foam volume. This paper presents further substantiation and verification of this approach based on the analysis of events statistics in fluctuating speckle patterns in comparison with the traditional approach based on the estimates of the correlation time of intensity fluctuations.

2. Experimental Technique and Results

2.1. Instrumentation and Experimental Technique

Experimental studies of dynamic scattering of laser radiation in evolving polymer foams were carried out using the previously described technique of depressurization-induced foaming of polylactic acid preliminary plasticized in the atmosphere of supercritical carbon dioxide [13–16]. Expanding D,L-polylactide foam in a multi-window high-pressure vessel was illuminated by a laser beam through the upper window and part of the scattered light was acquired by a high-performance CMOS-camera through the side window (Figure 1). The videos recorded by this camera were the sequences of speckle patterns changing from one frame to another; Figure 2a displays an example of a speckle-modulated frame arbitrarily chosen from the recorded video. Simultaneously with recording of a sequence of time-varying speckle patterns, the current images of expanding foam were recorded in the transillumination mode through another side window. Figure 2b shows a typical image of expanding foam; the recorded sequences of such images were used to recover the dependences of the current foam volume $V_f(t)$ on time.

In the experimental setup, a He-Ne laser (the output power is 2 mW, the wavelength is 633 nm, the linear polarization of outgoing beam) was used as a source of probe radiation. The video sequences of speckle patterns were recorded using the Optronis CamRecord camera + macro-lens assembly (4) with the frame rate of 60 or 100 fps (depending on the foam expansion rate). The design of high-pressure equipment used in the foaming procedure (in particular, a multi-window high-pressure vessel and the necessary appliances), as well as the rationale for the used materials, foaming modes, and image processing procedure for recovery of the current foam volume $V_f(t)$ were previously discussed in [15]. In the latter procedure, the current volume of expanding foam is considered as the volume of axisymmetric body with an axial cross section, determined by the corresponding image (see, for instance, Figure 2b). Dynamic scattering of probe laser radiation in the evolving polylactide foam was examined for the foaming modes with the initial pressure and temperature values ($P_{in} \approx 8.0$ MPa, $T_{in} \approx 40.0$ °C) near the corresponding critical values for carbon dioxide ($P_c \approx 7.3773$ MPa, $T_c \approx 30.9782$ °C, [17]). The choice of these initial conditions is due to the foaming efficiency (i.e., the ratio of the final volume of the foam to the volume of the plasticized polymer) is close to its maximal value [15]. Two depressurization modes were examined: a rapid pressure release with the average depressurization rate of ≈0.03 MPa/s, and slow depressurization with the rate of ≈0.006 MPa/s. Based on the previously obtained results [16], it can be assumed that a faster pressure release should lead to an increase in the degree of foam structure fragmentation compared to slow depressurization. In turn, this should manifest itself in the features of dynamic light scattering depending on the depressurization mode.

During recording of dynamic speckle structures by the camera (4), the gain parameter of the camera in the course of image capturing was selected in the preliminary experiments in such a way as to exclude saturation of the pixels in sequential captured images or to cause too low average value of pixel brightness in the sequential images. Accordingly, in further data processing, the current value of the speckle intensity at a given position in the image plane was assumed proportional to the current brightness of the corresponding pixel.

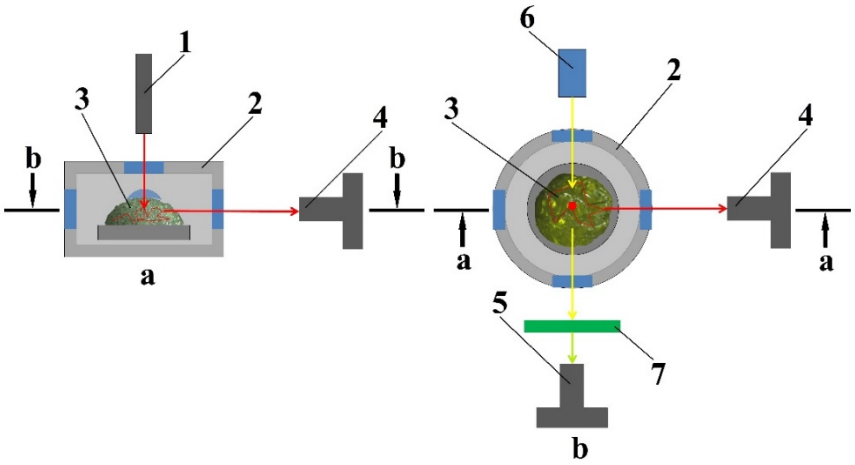

Figure 1. Schematic cross-sectional views of the experimental setup used for DLS probing of expanding polylactide foams; (**a**)–vertical section; (**b**)–lateral section. 1–a continuous-wave laser as a source of the probe beam; 2–a high-pressure multi-window vessel (reactor); 3–an expanding foam; 4–a high-performance CMOS camera with a macro-lens; 5–a CMOS camera for acquisition of the foam images; 6–a white-light illumination source for the camera (5); 7–a bandpass filter blocking laser radiation.

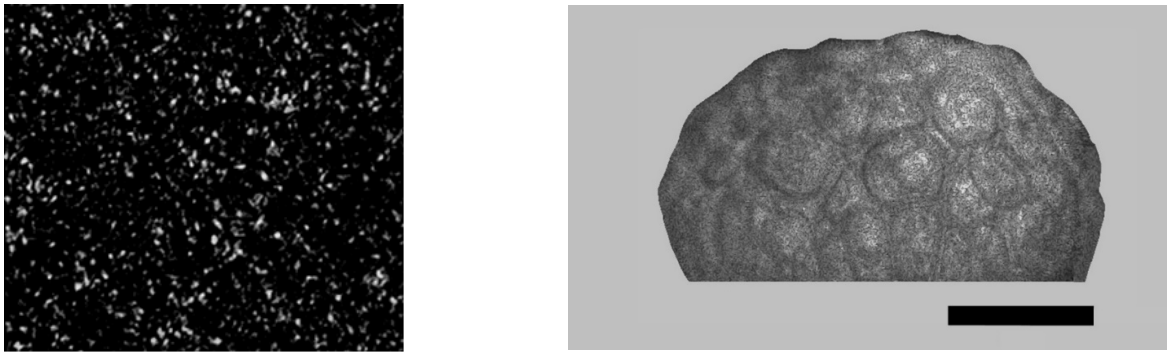

(**a**) (**b**)

Figure 2. (**a**) An example of a speckle-modulated frame captured by the camera (4); (**b**) A snapshot of the expanding polylactide foam captured by the camera (5); the image is processed to exclude insufficient details and noise; the black bar corresponds to 2 mm.

2.2. Analysis of the Time-Varying Speckle Patterns: Alternative Approaches

Two different approaches to the analysis of temporal dynamics of intensity fluctuations in the scattered laser radiation during foam expansion were examined. The first is based on the traditional estimate of the ensemble-averaged correlation time of intensity fluctuations. Due to pronounced nonstationarity of the scattering system in the course of its expansion, the captured image sequences were divided into non-overlapping fragments of a certain duration using a running window in the time domain. Calculation of correlation functions of intensity fluctuations for each fragment was carried out by averaging over both temporal and spatial coordinates:

$$\widetilde{g}_2(m) = \frac{1}{R}\sum_{r=1}^{R}\left\{\frac{\sum\limits_{k=1}^{K-m}\left(B_{k+m}^{r}-\langle B\rangle\right)\left(B_{k}^{r}-\langle B\rangle\right)}{\sum\limits_{k=1}^{K-m}\left(B_{k}^{r}-\langle B\rangle\right)^{2}}\right\}, \quad (1)$$

where index "r" defines a single pixel randomly selected in the sequence of frames, R is the number of randomly selected pixels used for ensemble averaging (in our case, R was set equal to 50). B_k^r is a gray-scale pixel brightness associated with the speckle pattern intensity at the r position for the k-th frame in the frameset selected by the running window, and $\langle B \rangle$ is the window- and ensemble-averaged brightness of pixels.

Duration of the fragments (i.e., the width of the running window) and window displacement along the time axis in the course of transition from one data analysis run to another were determined in the preliminary experiments. The main criterion for estimation of the window width and its step-by-step displacement along the time axis was based on the condition of insignificant changes in the evaluated correlation time (no more than 10%) during transition from one window position to another. It was found that, under the used foaming conditions, the acceptable fragment duration can be chosen equal to 10 s.

Another approach is based on the estimates of the average speckle lifetime within each time window of 10 s duration. These windows included 600 or 1000 captured frames (depending on the used frame rate of the camera 4). Figure 3 illustrates the image analysis procedure for evaluating the lifetime for an arbitrarily selected speckle within an arbitrarily selected frame in the window. In this procedure, a randomly selected speckle was tracked during their occurrence in the image plane. Accordingly, the selected speckle was tracked back in time until it appeared and forward in time until it disappeared. The appearance and disappearance moments were identified by the state of the speckle, when its brightness became less than 0.1 of the average frame brightnesss. The tracking was provided using a developed interactive MatLab procedure and taking into account the possible transverse displacements of speckles in the image plane. In Figure 3, k_{da} and k_a are the numbers of frames corresponding to the moments of speckle disappearance and appearance. Accordingly, the lifetime of a chosen speckle is equal to $\tau_{lt} = (k_{da} - k_a)/\Phi$, where Φ is the applied frame rate of CMOS camera (4). The average speckle lifetime $\langle \tau_{lt} \rangle$ was determined for ensembles of 20 randomly selected speckles which appeared and disappeared within the framesets selected at current positions of the running window.

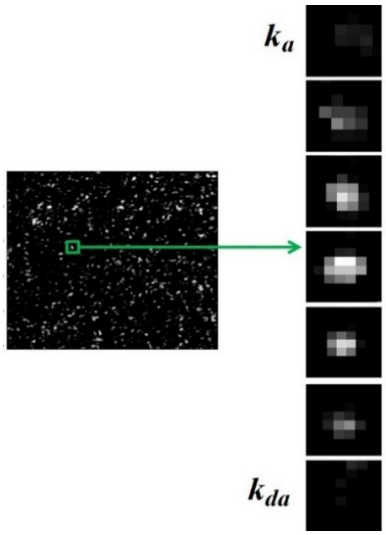

Figure 3. Illustration of the procedure for determining the lifetime of a speckle randomly selected in the frame.

2.3. Experimental Results

Figure 4 shows the examples of normalized autocorrelation functions $\widetilde{g}_2(\tau) = \widetilde{g}_2(m/\Phi)$ of intensity fluctuations obtained by processing of the sequences of speckle patterns within the ten-second time windows. It is necessary to point out a complex behavior of the recovered correlation functions caused by peculiarities of the dynamics of scattering sites in the evolving foams at the scale of the order of the probe light wavelength. The trends in their

behavior can be described within the framework of the frequently used simple analytical model of exponential decay $\widetilde{g}_2(\tau) \approx \exp(-\tau/\tau_c)$ only in the initial sections, which do not even cover one decade. At the same time, the correlation time of intensity fluctuations, determined from the decay of recovered functions $\widetilde{g}_2(\tau)$ to the $1/e$ level, monotonically increases as the foam expands.

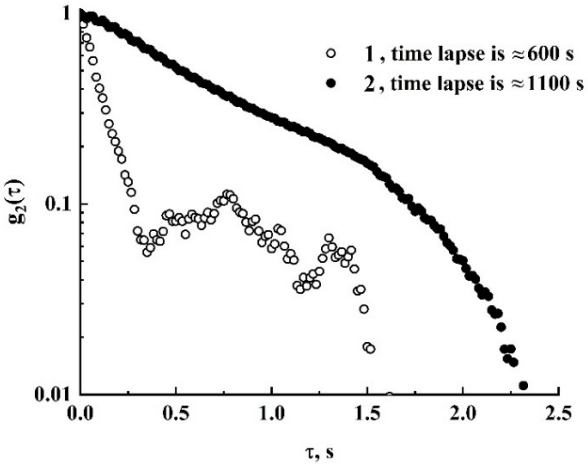

Figure 4. Examples of the recovered autocorrelation functions of speckle intensity fluctuations. The case of slow depressurization. The time lapse after beginning an intensive foam expansion: 1– ≈ 600 s; 2– ≈ 1100 s.

Similarly, the average lifetime of the speckles $\langle \tau_{lt} \rangle$ rises up when the foam volume V_f increases (Figure 5). The data presented in Figure 5 were obtained by averaging V_f and $\langle \tau_{lt} \rangle$ evaluated in a series of five foaming experiments carried out under the same conditions in cases of rapid and slow depressurization. Accordingly, the error bars characterize the scatter of the evaluated data for each series. A decrease in the foam expansion rate dV_f/dt at the final stage of foaming is accompanied by an expected abrupt increase in the average speckle lifetime, and vice versa. The relationship between V_f, dV_f/dt, and $\langle \tau_{lt} \rangle$ established in experiments are used for further interpretation of the relationship between the macroscopic and macroscopic dynamics of foam expansion, on the one hand, and dynamics of intensity fluctuations in the scattered laser radiation, on the other hand.

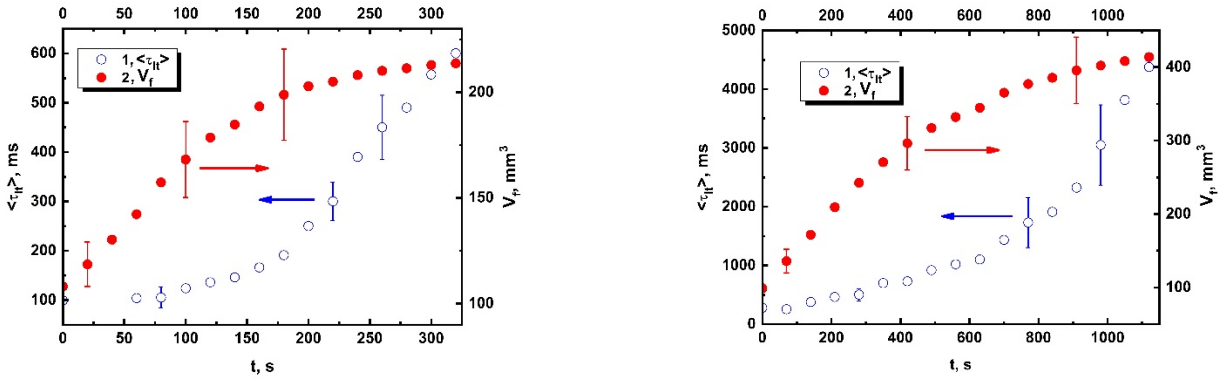

Figure 5. Current values of the average speckle lifetime (1) and the foam volume (2) against the time lapse in the course of intensive expansion of the polylactide foam. (**a**) Case of rapid depressurization; (**b**) case of slow depressurization. Zero time corresponds to transition from the nucleation stage to an intensive expansion of the foam. Selectively shown error bars correspond to a significance level of 0.9.

3. Correlation Analysis vs. Events Statistics Analysis of the Fluctuating Scattered Light: Comparative Study

3.1. Correlation Spectroscopy of Expanding Foams: Basic Principles and Modeling Results

The generally accepted approach to laser-based probing of microscopic dynamics in multiple scattering random media is diffusing-wave spectroscopy (or correlation spectroscopy) [18–20], which has been successfully applied over the past forty years to various time-varying objects, from sand flows to drying paints [21–23]. In particular, the applicability of diffusing-wave spectroscopy for characterizing microscopic dynamics in such multiple scattering random media as slowly evolving foams was considered in [20]. This technique is based on the correlation analysis of fluctuations in the intensity of laser radiation scattered by the probed object and detected using a single-point detection scheme or a multi-element detector (the multi-speckle technique, [24,25]). The main relationship of diffusing-wave spectroscopy has the following form (see, e.g., [26]):

$$g_1(t,\tau) = \exp(-j\omega\tau)\int_0^\infty \exp\left\{-\frac{1}{3}k_0^2\left\langle \Delta r^2(t,\tau)\right\rangle \frac{s}{l^*(t)}\right\}\rho(s,t)ds, \quad (2)$$

where $g_1(t,\tau) = \langle E(t)E^-(t+\tau)\rangle / |E(t)|^2$ is the normalized autocorrelation function of the light field fluctuations at the chosen observation point (the superscript "-" denotes the complex conjugation); $\rho(s,t)$ is the probability density function of the propagation paths s of statistically independent partial waves arriving at the observation point due to the sequences of multiple scattering events in the probed object; ω and k_0 are the frequency and wavenumber of the probe radiation; l^* is the transport mean free path of light propagation in the probed medium [27]. The $\left\langle \Delta r^2(t,\tau)\right\rangle$ value defines the ensemble-averaged squared displacement of the scattering sites over the time interval τ. The dependencies of $\rho(s,t)$, $l^*(t)$, and $\left\langle \Delta r^2(t,\tau)\right\rangle$ on the current time t characterize variations in optical and dynamic properties of the evolving probed medium.

Equation (2) is valid if the characteristic time spans of these variations are many times greater than the correlation time of light field fluctuations at the observation point. The factor $\exp(-j\omega\tau)$ has no effect on further analysis, and therefore will be omitted. The integral on the right-hand side of Equation (2) can be considered as an one-sided Laplace transform of the probability density function $\rho(s,t)$ with the parameter equal to $\left(k_0^2/3l^*\right)\cdot\left\langle \Delta r^2(t,\tau)\right\rangle$. In the experiments on dynamic light scattering, the analyzed object is the normalized autocorrelation function of intensity fluctuations, defined as $g_2(t,\tau) = \langle I(t)I(t+\tau)\rangle / \langle I(t)\rangle^2$ and related to $g_1(t,\tau)$ via the Siegert relation (see, e.g., [26]):

$$g_2(t,\tau) = 1 + \theta|g_1(t,\tau)|^2, \quad (3)$$

where $0 \le \theta \le 1$ is the parameter defined by detection conditions (ratio of the detector size to the characteristic size of the coherence area in the detection plane, or the average speckle size). If this ratio is close to 0, θ approaches to 1. In the opposite case of a large aperture of the detector significantly exceeding the average speckle size, θ tends to zero. For analysis, it is more convenient to use the autocorrelation function of unbiased values of intensity fluctuations:

$$\widetilde{g}_2(t,\tau) = \langle\{I(t) - \langle I(t)\rangle\}\{I(t+\tau) - \langle I(t)\rangle\}\rangle / \langle I(t)\rangle^2. \quad (4)$$

In the case of ideal detection conditions ($\theta = 1$), the Siegert relation reduces to the following form

$$\widetilde{g}_2(t,\tau) = |g_1(t,\tau)|^2. \quad (5)$$

Following from Equation (2), we can single out two key points in the consideration of the direct problem of diffusing-wave spectroscopy:

- description of microscopic dynamics of the scattering centers in the probed medium on spatial scale comparable to the wavelength of the probe light through definition of an adequate form of the term $\langle \Delta r^2(t,\tau) \rangle$;
- definition of an adequate form of the probability density function $\rho(s,t)$ for the used illumination and detection conditions.

Note that $\rho(s,t)$ corresponds to the time response $\widetilde{I}(t,\tau)$ of the medium when it is illuminated by an ultrashort light pulse for a given probe geometry: $\widetilde{I}(t,\tau) \to \widetilde{I}(t,s/v) \leftrightarrow \rho(t,s)$, where v is the group velocity of the probe radiation in the medium. Accordingly, describing the pathlength statistics $\rho(s,t)$ in the exact analytical form is almost impossible, with exception of some simple scattering geometries, and the most appropriate and commonly used way for solving this problem is to apply the Monte-Carlo simulation of the light transfer in the medium (see, e.g., [28]). Considering multiple scattering of a laser beam in the expanding foam (Figure 6), we can conclude that in this case the probability density $\rho(s,t)$ is a zero-valued magnitude in the region of small values of $s \le s_{th}(t)$, where the threshold value $s_{th}(t)$ at the moment is defined by the characteristic size of the foam $L(t)$.

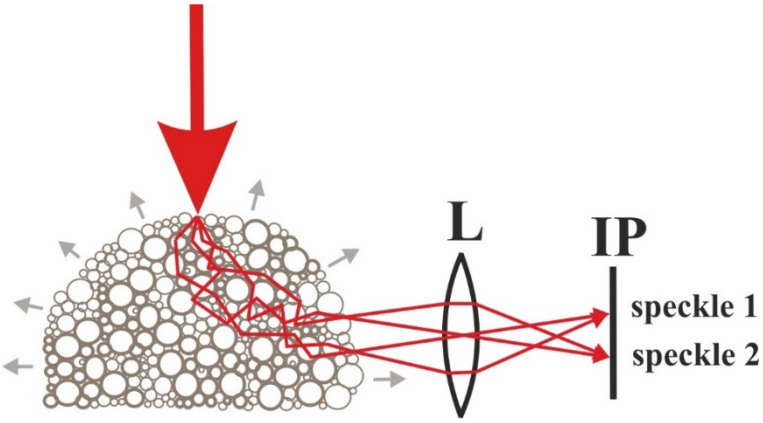

Figure 6. Model of multiple scattering of a laser beam (bold red arrow) in the expanding foam and formation of a speckle-patterned frame. *L* corresponds to the macro-lens of the camera 4 (Figure 1) and *IP* corresponds to the detection plane of the camera (4).

Note that the rate of decorrelation of scattered light fluctuations, determined by $\widetilde{g}_2(t,\tau)$, is strongly influenced by the ratio $L(t)/l^*(t)$. This ratio also affects the ensemble-averaged propagation path $\langle s(t) \rangle = \int_0^\infty s\rho(s,t)ds$(and, accordingly, the average number of scattering events) of the probing light in the medium. In the subsequent consideration, the relationship between the current values of the parameters L/l^* and $\langle s(t) \rangle / l^*(t)$, characterizing multiple scattering in the foam volume, and the decorrelation parameter $\widetilde{S}_c$ of scattered light fluctuations was analyzed using the results of the Monte Carlo simulations. The parameter $\widetilde{S}_c$ was estimated as the value of $\widetilde{S} = k_0^2 \langle \Delta r^2(t,\tau) \rangle / 3l^*(t)$ corresponding to the $1/e$ decay of $\widetilde{g}_2\left(t,\widetilde{S}\right)$(see Equations (2) and (5)). In the subsequent consideration, we will assume that the changes in the parameters L and l^* during the time interval, which is required for $\widetilde{S}_c$, $\langle s \rangle$ estimates, can be neglected. Therefore, the time variable t will be excluded when writing subsequent expressions. In the simulation, the shape of the expanding foam was assumed to be close to hemispherical, and the laser beam fell onto the polar region of the hemisphere (Figure 6). The multiple scattered partial components of the light field associated with photons in the Monte Carlo procedure were collected for the directions near the equatorial plane of the hemisphere, which correspond to the aperture angle of the used macro-lens. This configuration was consistent with the illumination and detection geometry used in the experiment. The modeled foam was assumed to be a non-absorbing multiple scattering medium with close-to-isotropic scattering; its effective refractive index was set equal to the refractive index of the surrounding space. Applicability

of the latter assumption follows from consideration of the foam as a two-phase cellular structure consisting of gas-filled cells; the volume fraction of the polymer phase in the foam is relatively small. Accordingly, we can assume that effect of multiple reflections of diffusing partial components from the space-foam interface back into the foam volume is relatively insignificant.

The simulation was carried out in accordance with the following procedure: at the first stage, the ensemble $\{s_i\}$ of random values of the propagation paths was generated and the sample probability density function $\rho(s)$ was recovered for the given values of l^* and L (the characteristic size L of the foam was accepted equal to the hemisphere radius). The sample size of $\{s_i\}$ for each simulation run was equal to 10^7, and the bin sizes during $\rho(s)$ recovery were chosen equal to $\Delta s = (s_{\max} - s_{\min})/1000$, where $s_{\max}, s_{\min}$ are the maximal and minimal pathlength values obtained in the given simulation run. Then, a set of $\left\{\widetilde{g}_2\left(\widetilde{S}_{(k)}\right)\right\}$ was recovered for a sequence of equidistant values $\left\{\widetilde{S}_{(k)}\right\}$ in accordance with the following expression:

$$\widetilde{g}_2\left(\widetilde{S}_{(k)}\right) = \sum_{p=0}^{P-1} \exp\left\{-\widetilde{S}_{(k)}\Delta s\left(\frac{1}{2}+p\right)\right\}\widetilde{N}_p,\ \widetilde{S}_{(k)} = \{0, 0.1\Delta s, 0.2\Delta s, \ldots, k\Delta s, ..\}. \quad (6)$$

Here, $\widetilde{N}_p$ are the weighted numbers of counts in the bins obtained during the frequency count analysis of the obtained datasets $\{s_i\}$ ($\sum_{p=0}^{P-1} \widetilde{N}_p = 1$), $P = 1000$ is the applied number of bins. The decorrelation parameter $\widetilde{S}_c$ is then evaluated for the given dataset $\{s_i\}$. In addition to $\widetilde{S}_c$, the average pathlengths $\langle s \rangle$ were also assessed as

$$\langle s \rangle = \sum_{p=0}^{P-1} \Delta s\left(\frac{1}{2}+p\right)\widetilde{N}_p. \quad (7)$$

Figures 7 and 8 illustrate the main features in the behavior of the obtained model data. Figure 7, a displays examples of the obtained sample probability density functions $\rho(s)$ for various values of the ratio s/l^*.

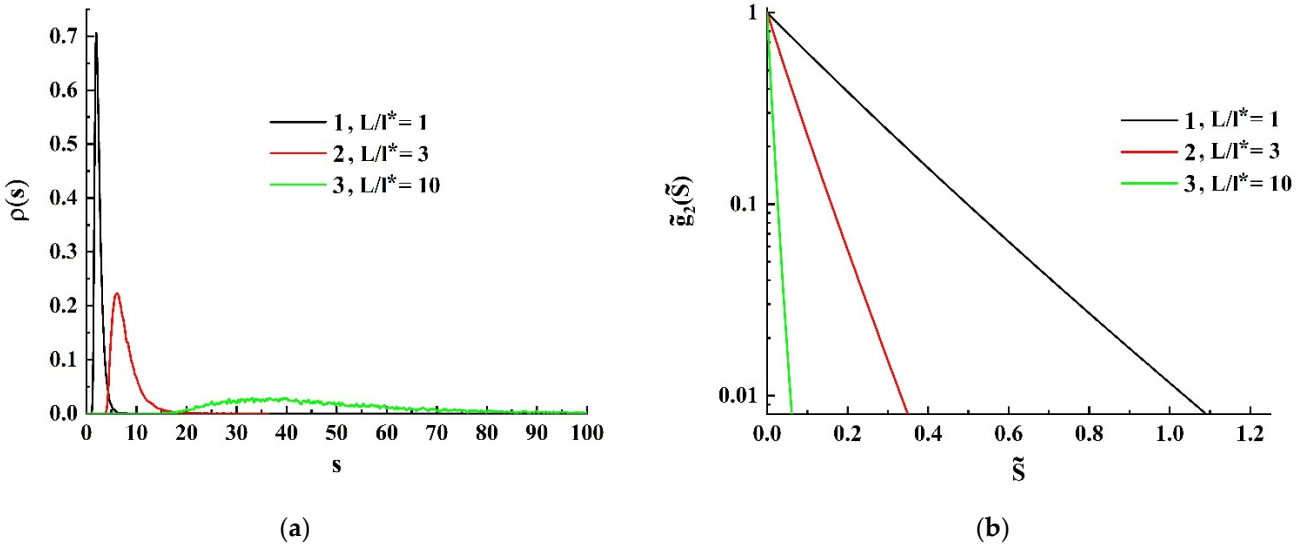

Figure 7. (**a**) The model probability density functions $\rho(s)$ (the s values are given in units of the transport mean free path l^*) for the foams with various ratios L/l^*; 1–$L/l^* = 1$; 2–$L/l^* = 3$; 3–$L/l^* = 10$. (**b**) The corresponding model autocorrelation functions of speckle intensity fluctuations.

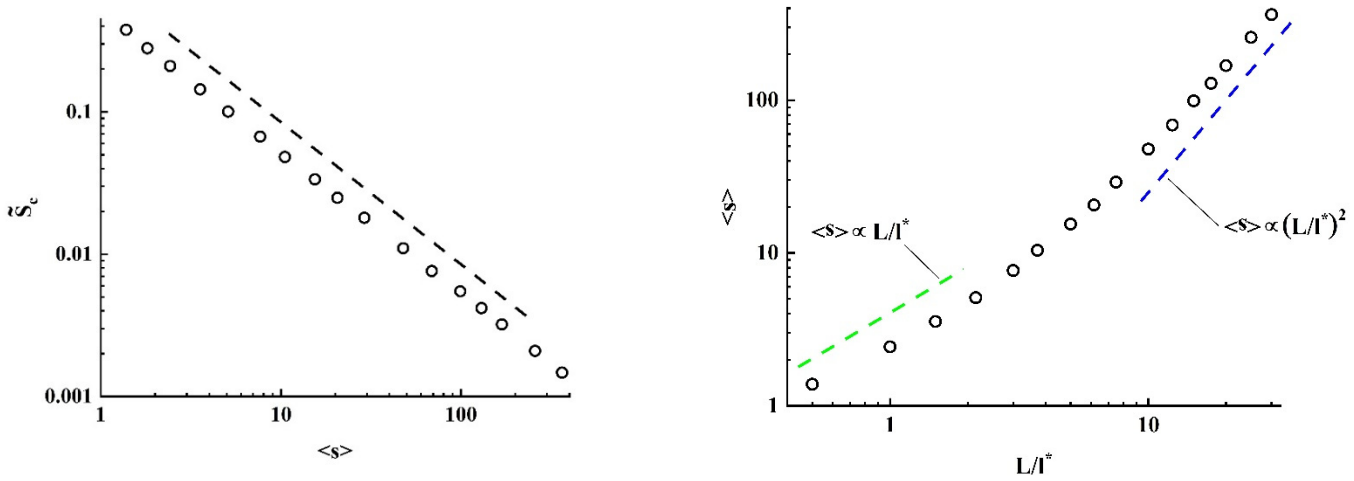

(**a**) (**b**)

Figure 8. (**a**) Model values of the decorrelation parameter against the average pathlength of probe radiation in the foam. The dashed line indicates an inverse linear relationship between $\widetilde{S}_c$ and $\langle s \rangle$ serves as a guide to the eye. (**b**) The average pathlength $\langle s \rangle$ (in units of the transport mean free path) in the model foam depending on the ratio L/l^*.

The general property of the obtained model probability density distributions is their localization in a limited region of the s domain; typically, substantially non-zero values $\rho(s)$ occupy the interval of s values with a length comparable to $\langle s \rangle$ due to confinement of the sequences of scattering events in the probed volume. In turn, this causes a close-to-exponential decay of the model autocorrelation functions $\widetilde{g}_2\left(\widetilde{S}\right)$ (Figure 7b). This feature is due to the abovementioned localization of the probability density distributions $\rho(s)$ for the discussed scattering geometry. Indeed, considering the extreme case of localization of the pathlength probability density distributions $\rho(s) \propto \delta(s - s')$, we arrive at the following relationship (see Equation (2)):

$$|g_1(\tau)| \to \exp\left(-\frac{1}{3}k_0^2\left\langle \Delta r^2(\tau)\right\rangle \frac{s'}{l^*}\right). \tag{8}$$

Here, $\delta(s - s')$ is the delta-function. Accordingly, we should expect a close-to-exponential decay of $\widetilde{g}_2\left(\widetilde{S}\right)$ due to confinement of multiple scattering in the modeled foam. In addition, an approximately inverse linear dependence of the model decorrelation parameter $\widetilde{S}_c$ on the average pathlength normalized by the transport mean free path l^* should be mentioned (Figure 8a). At the same time, the relationship between the average path $\langle s \rangle$, which directly determines the average number of scattering events in the probed medium, and the characteristic volume size L exhibits different trends depending on the ratio L/l^*. These trends are illustrated by the colored dashed lines in Figure 8b drawn as the guides for the eye (the green line corresponds to the approximately linear relationship $\langle s \rangle \propto L/l^*$ in the region of small L/l^* values, and the blue line marks the quadratic trend $\langle s \rangle \propto (L/l^*)^2$ occurring with an increase in L/l^*. Taking into account that the average number of scattering events $\langle N_{sc} \rangle$ in the probed volume is directly proportional to $\langle s \rangle$ ($\langle N_{sc} \rangle \propto \langle s \rangle / l \propto \langle s \rangle / (1 - g) l^*$, where l is the scattering mean free path and g is the scattering anisotropy parameter, see, e.g., [26]), we can conclude that $\langle N_{sc} \rangle \propto L/l^*$ in the low-step scattering mode. With the transition to the diffusion mode of probe light propagation, the relationship between $\langle N_{sc} \rangle$ and L/l^* approaches the quadratic law $\langle N_{sc} \rangle \propto (L/l^*)^2$.

Note that these model trends fairly agree with the remarks of D. Weitz and D. Pine ([26], p. 672) regarding the influence of the scattering medium size on the average number of scatterings of probe radiation in a medium. The decorrelation parameter $\widetilde{S}_c$ is directly related to the mean square $\left\langle \Delta r^2(\tau_c)\right\rangle$ of the scatter displacement during the correlation time

τ_c of intensity fluctuations through the relationship $\left\langle \Delta r^2(\tau_c) \right\rangle = 3l^* \widetilde{S}_c / k_0^2$. Accordingly, it seems feasible to determine an ensemble-averaged characteristic of the microscopic scatter mobility in the probed volume from the experimentally measured value τ_c. However, the key point in this approach is the need for *a priori* information about the type of microscopic dynamics of scattering sites in the medium. In particular, the classical Brownian motion of scattering particles gives $\left\langle \Delta r^2(\tau) \right\rangle \propto \tau$ with the proportionality coefficient determined by the translational diffusion coefficient of particles ($\mu m^2/s$); in the case of the dominant drift-like motion of particles $\left\langle \Delta r^2(\tau) \right\rangle \propto \tau^2$ with the proportionality coefficient associated with the squared drift velocity of the scattering sites ($\mu m^2/s^2$). The most complex case is the combination of generalized Brownian dynamics and drift of particles: $\left\langle \Delta r^2(\tau) \right\rangle \propto C_1 \tau^\gamma + C_2 \tau^2$, where the exponent γ has the value between 0 and 2, and the parameters C_1, C_2 relate to contributions of diffusion and drift-like motions to the mobility of scatterers. In addition, in rapidly evolving systems (for example, in expanding foams), significant changes in the type of microscopic dynamics of the structure are eventual in the course of evolution.

Thus, a lack of precise *a priori* knowledge about the nature of microscopic dynamics of particles in the medium when assessing parameters of microscopic mobility from the correlation time τ_c will most likely lead to their ill-conditioned estimates. In this regard, in the next subsection we will consider an alternative approach to the analysis of fluctuations of scattered light, which seems to be free from the mentioned pitfall.

3.2. Events Statistics Analysis of Fluctuating Scattered Light

This alternative approach to characterizing dynamic speckles is based on the time-frequency analysis of certain events in the evolving speckle field. As such events, we can consider, for example, transitions of the current values of speckle intensity at various points of the observation plane through a certain threshold value (the threshold level crossings). From general considerations, it can be assumed that the number of such events per unit time and unit area in the observation plane (the rate of events) should correlate with the parameters of microscopic mobility of scattering centers in the probed medium. In particular, the characteristic time of mutual displacements of scattering centers at the distance equal to the wavelength of probe radiation is one of the key characteristics of the microscopic scatter mobility. The threshold level, which determines the moments of event occurrence, should in a certain way relate to the average intensity of the speckle field for the analyzed time interval: $I_{th} = K\langle I \rangle$, where K is the dimensionless threshold level. In the further consideration, we will analyze two model parameters of the observed dynamic speckle field, determined by the dynamics of stochastic phase modulation of partial light waves forming the evolving speckle field. These parameters are the average rate of crossing events $\left\langle \dot{N} \right\rangle$ for an arbitrarily chosen observation point and the average speckle lifetime $\langle \tau_{lt} \rangle$. The latter parameter can be defined as the residence time of intensity of an individual speckle above the threshold level I_{th}, averaged over the speckle ensemble.

At the first stage of modeling, we will consider formation of the evolving speckle field at an arbitrarily chosen observation point within the framework of the discrete scattering model widely used in statistical optics (see, e.g., [29,30]). In this case, the current value of the observed intensity I_k at the k-th simulation step can be written as follows

$$I_k \propto \left| \sum_i^{N_i} E_i \exp\{-j(\varphi_{i0} + \Delta\varphi_{ik})\} \right|^2, \tag{9}$$

where E_i is the amplitude of the i-th partial wave incoming at the observation point from a probed random system of scatterers, φ_{i0} is its initial phase, and $\Delta\varphi_{ik}$ is the corresponding phase shift accumulated over k simulation steps. All N_i waves interfering at the observation point are assumed to be statistically independent and have equal amplitudes. Without loss of generality in further consideration, we can set all the amplitudes E_i equal to 1. Depending on the scenario of changing the phase shifts $\Delta\varphi_{ik}$ when going from k-th to

$(k+1)$-th simulation step, we should expect different cases of fluctuation dynamics of the intensity I_k at the observation point. Two extreme cases were considered during the simulation: (1) when $\Delta\varphi_{ik} = \xi_i k$, and (2) when $\Delta\varphi_{ik+1} - \Delta\varphi_{ik} = \xi_{ik}$, where ξ_i and ξ_{ik} are the statistically independent magnitudes randomly distributed between $-\pi \cdot F_\xi$ and $\pi \cdot F_\xi$ with the zero mean values (F_ξ is the scale factor used in the simulation procedure). It should be noted that the variance of the phase shifts $\sigma^2_{\Delta\varphi(k)}$ varies with k (i.e., with time) in the first case as $\sigma^2_{\Delta\varphi(k)} = \sigma^2_\xi k^2$, while in the second case as $\sigma^2_{\Delta\varphi(k)} = \sigma^2_\xi k$ (here σ^2_ξ is the variance of the phase shift increments).

Accordingly, case (1) can be interpreted as corresponding to the "drift-like" dynamics of changes in the phases of random phasors corresponding to the interfering waves. On the contrary, case (2) corresponds to the "diffusion-like" dynamics of phase shifts. For the considered scenarios of changes in $\sigma^2_{\Delta\varphi(k)}$ depending on k, the qualitative differences in the dynamics of simulated fluctuations of speckle intensity are illustrated by Figure 9. Note that the value of $F_\xi = 0.01$ is assumed the same in both cases, and the values of phase shifts ξ per single simulation step are assumed as uniformly distributed random variables. Consequently, σ^2_ξ is related to the introduced scale factor as $\sigma^2_\xi = \pi^2 F^2_\xi / 3$.

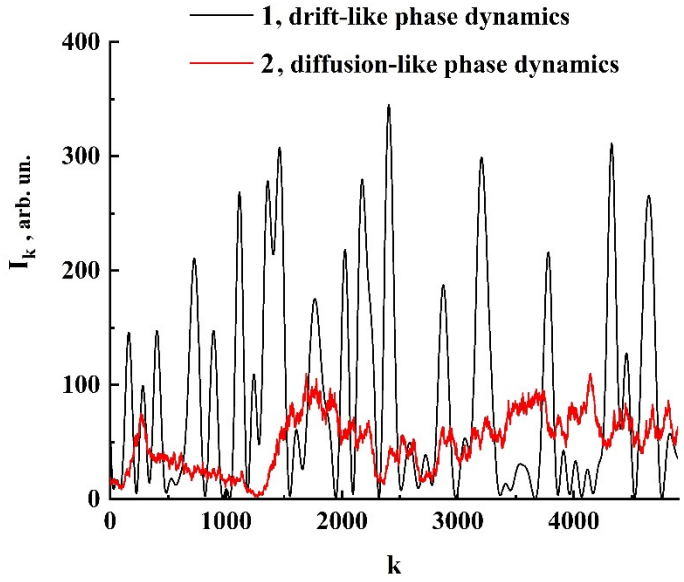

Figure 9. Fragments of the model time series of intensity fluctuations in cases (1) and (2).

The normalized autocorrelation functions of the simulated intensity fluctuations were calculated as:

$$\widetilde{g}_2(m) = \sum_{k=0}^{\widetilde{K}-M} (I_{k+m} - \langle I \rangle)(I_k - \langle I \rangle) / \sum_{k=0}^{\widetilde{K}-M} (I_k - \langle I \rangle)^2, \quad (10)$$

where the upper values of m (M), during the calculation of $\widetilde{g}_2(m)$, were set significantly smaller in comparison with the numbers of terms $\widetilde{K}$ in the corresponding sequences $\{I_k\}$ obtained as a result of the simulation runs. In our case, $\widetilde{K}$ was taken equal to 10^7 and M was set equal to 1×10^6. The number of statistically independent interfering waves, or random phasors N_i in Equations (9) and (10) was taken equal to 100. The model autocorrelation functions $\widetilde{g}_2(m)$ calculated for the drift-like and diffusion-like dynamics of phase shifts are displayed in Figure 10a,b.

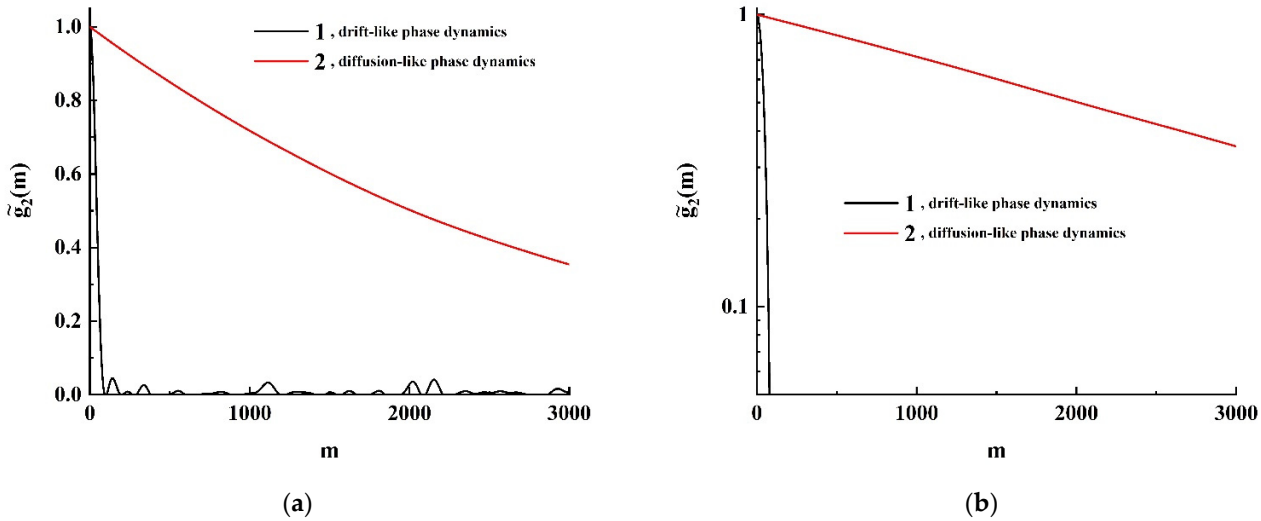

Figure 10. Modeled autocorrelation functions of intensity fluctuations in the linear (**a**) and semi-logarithmic (**b**) coordinates; 1–"drift-like" dynamics of accumulated phase shifts; 2–"diffusion-like" dynamics. Note a dramatic difference in the correlation times of intensity fluctuations in the cases (1) and (2).

It is clearly seen that autocorrelation functions of intensity fluctuations in cases 1 and 2 demonstrate completely different trends in decay with the increasing m lag: pure exponential decay in the case of "diffusion-like" dynamics of phase increments (2), and stretched exponential decay in the case of "drift-like" dynamics (1). Additionally, the correlation time of intensity fluctuations increases significantly faster with the decreasing F_ξ (and, accordingly, σ_ξ) in case 2 compared to the case of "drift-like" dynamics: $m_{c,2} \propto F_\xi^{-2}$ against $m_{c,1} \propto F_\xi^{-1}$ (here, $m_{c,1,2}$ are the values of the correlation time expressed in the numbers of simulation steps). Thus, the presence or absence of a stable trend ("memory effect") in the evolution of phase shifts of interfering partial waves (random phasors) dramatically affects the correlation time at the same values of σ_ξ per one modeling step (or the rate $\dot{\sigma}_\xi$ of the ensemble-averaged phase shift in the case of continuous time).

On the contrary, based on the simulation results obtained, it can be assumed that the proposed estimates of event flux density in the analyzed speckle patterns are invariant with respect to the type of dynamics of phase fluctuations in interfering partial waves. The sequences $\{I_k\}$ obtained in the cases 1 and 2 for various values of the scale factor F_ξ were processed for establishing the relationship between the simulated values of the average speckle lifetime $\langle \tau_{lt} \rangle$ and the average rate of crossing events $\left\langle \dot{N} \right\rangle$ and the dimensionless threshold level K. Figure 11 displays the simulated values $\langle \tau_{lt} \rangle$ and $\left\langle \dot{N} \right\rangle$ against F_ξ for the various values of K in the range from 0.1 to 2.1; the average speckle lifetimes are expressed in terms of the number of simulation steps; the average rates of crossings are related to one simulation step.

The inverse linear relationship between $\langle \tau_{lt} \rangle$ and F_ξ ($\langle \tau_{lt} \rangle \approx A_{1,2}(K)/F_\xi$) and the linear relationship between $\left\langle \dot{N} \right\rangle$ and F_ξ ($\left\langle \dot{N} \right\rangle \approx B_{1,2}(K)F_\xi$) are obvious; also note the close values of the constants A and B for both extreme cases in the dynamics of phase fluctuations. Insignificant discrepancies between A_1, A_2 and B_1, B_2 are presumably due to intrinsic limitations of the modeling procedure (the finiteness of data sequences and their discreteness). Figure 12 displays the values of these constants against K. Selectively shown error bars characterize the spread of A and B values over a series of 10 statistically independent simulation runs. At first glance, such an invariance of $\langle \tau_{lt} \rangle$ and $\left\langle \dot{N} \right\rangle$ with respect to the type of dynamics of phase fluctuations compared to the correlation time of intensity fluctuations seems surprising. However, this fundamental feature is because $\langle \tau_{lt} \rangle$ and $\left\langle \dot{N} \right\rangle$ are related to the *first-order*, or single-point, statistics of intensity of scattered

waves and are determined by the probability density function $\rho(I_k)$. At the same time, the correlation time τ_c is a parameter related to the *second-order*, or two-point statistics of intensity fluctuations.

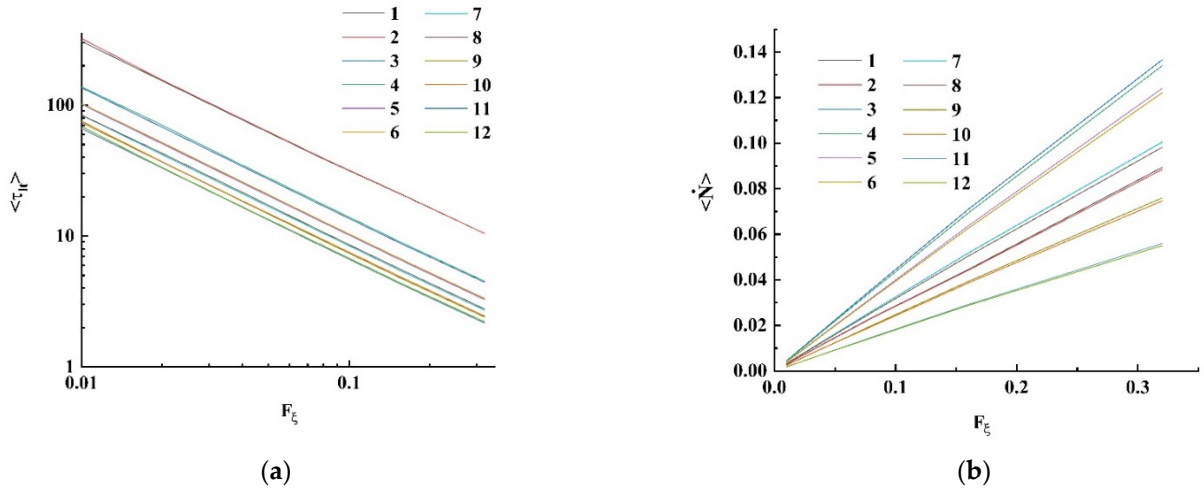

(**a**) (**b**)

Figure 11. Model dependencies of $\langle\tau_{lt}\rangle$ (**a**) and $\langle\dot{N}\rangle$ (**b**) on F_ξ for various threshold levels; case 1–(1–6), case 2–(7–12); the threshold levels are: 0.1 (1, 7); 0.5(2, 8); 0.9 (3, 9); 1.3 (4, 10); 1.7 (5, 11); 2.1 (6, 12).

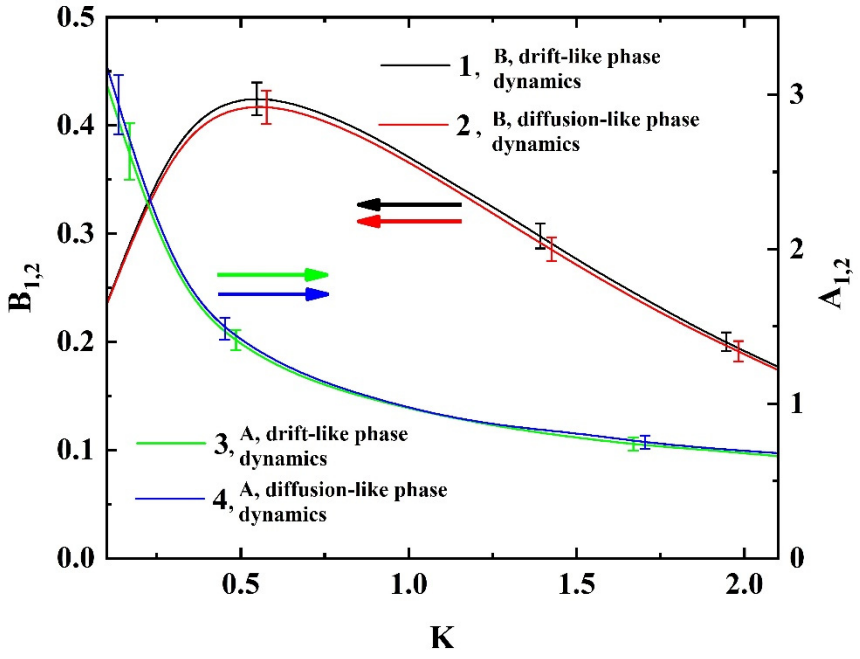

Figure 12. Model dependencies of the scaling parameters $A_{1,2}$ and $B_{1,2}$ on the normalized threshold level K. 1–B_1; 2–B_2; 3–A_1; 4–A_2. Selectively shown error bars correspond to a significance level of 0.9.

Considering the case of multiple scattering of the propagating partial waves, it is necessary to take into account that the values of phase shifts $\Delta\varphi_{ik}$ for random phasors in Equation (9) are the result of accumulation of local phase shifts. These local phase shifts occur in statistically independent single scattering acts, resulting in a random sequence of scattering acts for each partial wave associated with a random phasor. Applying the hypothesis of statistical independence of local phase shifts and based on the central limit theorem,

we can arrive to the following ensemble-averaged relationship between the variance of local phase shifts and the resulting variance of phase shifts for a set of random phasors:

$$\sigma_{\xi}^{2} = \langle N_{sc} \rangle \left(\sigma_{\xi}^{s}\right)^{2}, \tag{11}$$

where $\langle N_{sc} \rangle$, as before, is the ensemble-averaged number of scattering events for an ensemble of interfering partial waves and $\left(\sigma_{\xi}^{s}\right)^{2}$ is the ensemble-averaged phase shift variance per single scattering event. Accordingly,

$$\sigma_{\xi} = \langle N_{sc} \rangle^{0.5} \sigma_{\xi}^{s}. \tag{12}$$

Note that the value of σ_{ξ}^{s} is directly related to an ensemble-averaged displacement of scattering sites per single simulation step.

4. Discussion of the Results

In further consideration, we need to derive a relation between the microscopic dynamics of interphase boundaries in the expanding foam and the current volume of foam measured in the experiments. The relationship between the volume-averaged characteristic of microscopic dynamics in the foam and the foam expansion rate dV_f/dt can be established using the expression for the average cell size in the foam:

$$\langle D \rangle = \left(\frac{K_c V_f}{N_c}\right)^{\frac{1}{3}}, \tag{13}$$

where K_c is the scale factor defined by the ensemble-averaged shape of cells (in particular, $K_c \approx 6/\pi$ in the case of near-spherical cells) and N_c is the number of cells in the foam volume. Accordingly, the increment of $\langle D \rangle$ during the time interval Δt can be represented as:

$$\Delta \langle D \rangle \approx \left\{ \left(\frac{K_c V_f}{N_c}\right)^{\frac{1}{3}} \right\}' \Delta t = \frac{K_c^{\frac{1}{3}}}{3} \left\{ \left(\frac{V_f}{N_c}\right)^{-\frac{2}{3}} \left(\frac{V'_f N_c - V_f N'_c}{N_c^2}\right) \right\} \Delta t. \tag{14}$$

Here, we assume that $V_f(t)$ and $N_c(t)$ are monotonically varying differentiable functions of time. On the other hand, the ensemble-averaged magnitude of stochastic phase modulation of partial components of laser radiation in the foam volume per scattering event can be estimated as follows. The scattering centers in the expanding foam are cell walls, zones of wall intersections (so-called Plateau-Gibbs channels), and nodes of a stochastic three-dimensional grid of the Plateau-Gibbs channels. Optical transport parameters (the scattering mean free path l and transport mean free path l^*, [27]) for this scattering system can be expressed in terms of the current values of $\langle D \rangle$.

Following D. Durian with co-workers [31], we can assume that the following relation holds in foam-like systems: $l, l^* \propto \langle D \rangle$. Keeping in mind that the scattering mean free path is interpreted as the average propagation length of partial components between sequential scattering events, it can be assumed that the above introduced ensemble-averaged phase shift σ_{φ} per single scattering event during the time interval Δt is proportional to $\Delta \langle D \rangle$: $\sigma_{\varphi} \propto (2\pi/\lambda)\Delta \langle D \rangle$. In accordance with the simulation results presented in Section 3.2, we can write the following relationship between the total critical phase shift $\Sigma_{\varphi}^{I_{th}}$ at a given threshold and the average speckle lifetime $\langle \tau_{lt} \rangle$: $\Delta t = \langle \tau_{lt} \rangle \rightarrow \langle N_{sc} \rangle^{0.5} \sigma_{\varphi} = \Sigma_{\varphi}^{I_{th}}$. On the other hand, the average number of scattering events is determined by the ratio of the characteristic size of the scattering medium $L \propto \left(V_f\right)^{\frac{1}{3}}$ to the transport mean free path $l^* \propto \langle D \rangle$. Accordingly, we arrive at the following semi-quantitative relation for $\langle N_{sc} \rangle$:

$$\langle N_{sc} \rangle \propto \left(\frac{L}{l^*}\right)^{\beta} \propto (N_c)^{\frac{\beta}{3}}, \tag{15}$$

where the exponent β, as has been established in the Section 3.1, is close to 1 in the low-step-scattering mode and approaches 2 when the ratio L/l^* increases above 5 ÷ 6 (see Figure 8b). Thus, we finally obtain the basic semi-quantitative relationship for the case of dynamic light scattering probes of the expanding foam using evaluation of the average speckle lifetime:

$$\langle \tau_{lt} \rangle \propto (N_c)^{-\frac{\beta}{6}} \left(\frac{V_f}{N_c} \right)^{\frac{2}{3}} \left(\frac{N_c^2}{V'_f N_c - V_f N'_c} \right) = (N_c)^{\frac{2-\beta}{6}} \left(V_f \right)^{\frac{2}{3}} \left(\frac{1}{V'_f - \left(V_f / N_c \right) N'_c} \right). \quad (16)$$

Equation (16) clearly describes the experimentally observed tendency (Figure 5) to an increase in the average speckle lifetime with an increase in the foam volume and decrease in the volume change rate. In the case of a constant number of cells in the volume of the expanding foam, $N_c = const$, this equation reduces to the following relation $\langle \tau_{lt} \rangle \propto \left(V_f \right)^{\frac{2}{3}} \left(1/V'_f \right)$. Figure 13 displays the experimentally obtained average speckle lifetimes $\langle \tau_{lt} \rangle$ against the values of $\Upsilon = \left(V_f \right)^{\frac{2}{3}} \left(1/V'_f \right)$ recovered from the empirical dependencies $V_f(t)$ for two examined depressurization modes (Figure 5). The uncertainties in evaluation of the average speckle lifetimes and the parameter Υ, which are characterized by the error bars in Figure 13, relate to the experimental errors displayed in Figure 5.

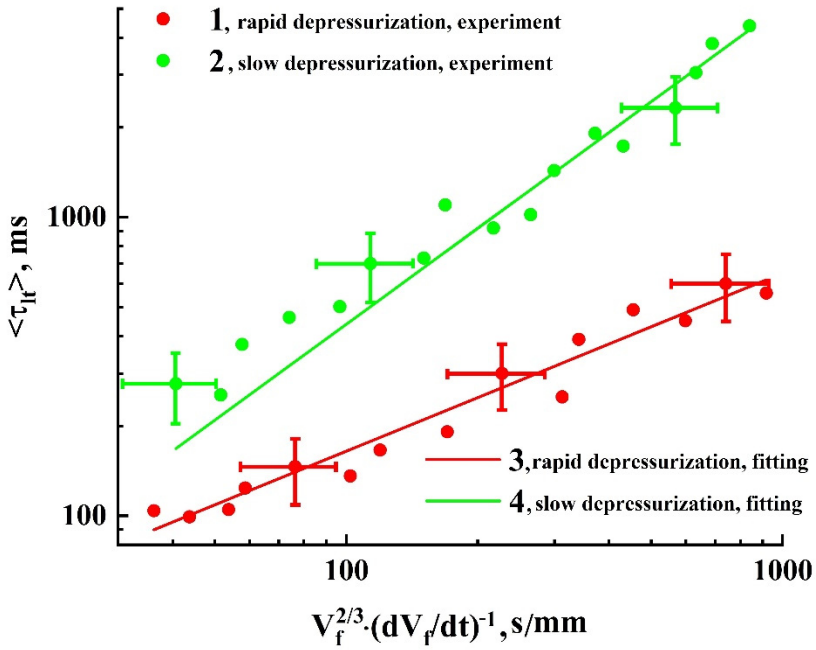

Figure 13. 1, 2–dependencies of the average speckle lifetime on $\Upsilon = \left(V_f \right)^{\frac{2}{3}} \left(1/V'_f \right)$ recovered from experimental data for the cases of rapid (1) and slow (2) depressurization; 3, 4–results of fitting the recovered data with the power-law dependencies $\langle \tau_{lt} \rangle \propto \Upsilon^{\delta}$. Selectively shown error bars correspond to a significance level of 0.9.

Note that the relationship between $\langle \tau_{lt} \rangle$ and $\left(V_f \right)^{\frac{2}{3}} \left(1/V'_f \right)$ in the case of slow depressurization admits, with acceptable accuracy, a linear approximation (the green solid line in Figure 13, $\langle \tau_{lt} \rangle \approx (4.22 \pm 1.42) \cdot \Upsilon^{(1.02 \pm 0.07)}$). At the same time, an increase in the rate of pressure release during foaming leads to a remarkable deviation in the dependence of the average speckle lifetime on the introduced parameter $\left(V_f \right)^{\frac{2}{3}} \left(1/V'_f \right)$ from the linear trend (the dataset 1 and the red fitting line $\langle \tau_{lt} \rangle \approx (11.56 \pm 3.30) \cdot \Upsilon^{(0.59 \pm 0.05)}$ in Figure 13). This feature can be interpreted in terms of effect of a variable number of cells $N_c(t)$ in

accordance with the Equation (16). Previous experimental studies of the foaming mode effect in the atmosphere of supercritical carbon dioxide on the structure of the formed highly porous polylactide matrices (see, e.g., [16]) clearly show that an increase in the depressurization rate leads to an increase in fragmentation of the matrix structure. In addition, rapid depressurization is characterized by lower foaming efficiency, described in terms of the ratio of the final foam volume to the initial polymer volume [15]. This indicates that during rapid foaming, a larger fraction of internal energy of the foaming agent is spent, in particular, on formation of interphase boundaries in the foam volume, as compared to the case of slow pressure release. Thus, it should be expected that a rapid depressurization mode is characterized by a remarkable increase in the number of cells in the foam volume with time span. Note that an increase in the number of cells in the foam as it expands has a double effect on the examined time parameters of intensity fluctuations of the scattered laser light. On the one hand, an increase in N_c leads to a decrease in the ensemble-averaged mobility of the scattering sites, considered in terms of the changes in $\langle D \rangle$ during the time interval Δt (Equation (14)). On the other hand, an increasing number of cells in the foam volume should provoke an increase in the average number of scattering events $\langle N_{sc} \rangle$ in the course of probe light propagation in the foam volume and, accordingly, a decrease in the average speckle lifetime. However, the latter effect is expected to be rather subtle due to small values of the exponent $\beta/6$. Considering Equation (14), we can see that the increase in the number of cells over time partially reduces the influence of the term V'_f due to positive values of the term $\left(V_f/N_c\right)N'_c$. Consequently, the values of $\langle \tau_{lt} \rangle$ in the case of rapid depressurization exhibit a slower increase with increasing of $\left(V_f/N_c\right)N'_c$, being significantly smaller than the average speckle lifetimes under a slow pressure release. Note that the intervals of changes in the $\langle \tau_{lt} \rangle$ values in Figure 13 correspond in both cases to a complete stage of intensive foam expansion (compare with Figure 5). The established trends in the behavior of the dependences of the average speckle lifetime on Υ ($\langle \tau_{lt} \rangle \propto \Upsilon^{0.59}$ (1) and $\langle \tau_{lt} \rangle \propto \Upsilon^{1.02}$(2)) are manifested in a wide range of Υ, beginning from ≈40 s/mm (transition from nucleation to intensive foam expansion) to ≈1000 s/mm (transition to stabilization of the foam structure). Thus, smaller value of the exponent in the approximating power-law dependences of $\langle \tau_{lt} \rangle$ on Υ in the case of rapid depressurization is observed during the entire stage of intensive foam expansion.

5. Conclusions

Thus, the examined approach to the analysis of dynamic scattering of laser radiation in rapidly evolving media with a complex structure has such an advantage as absence of the need for *a priori* information relating the features of the stochastic phase modulation dynamics of the probe light at the microscopic level. This approach can be identified as the event statistics analysis and involves the use of informative parameters associated with estimation of the ensemble-averaged frequency of the crossings of a given threshold level by the fluctuating speckle intensity during a selected time interval. In particular, the introduced average speckle lifetime characterizes the ensemble-averaged time for the speckle intensity to take up the residence above the threshold level. Invariance of event statistics parameters with respect to the type of dynamics of phase fluctuations of scattered radiation, established by simulation, follows from the fact that the frequency of level crossings refers to the *first-order* statistics of speckle intensity. In the case of multiple scattering of laser radiation in the medium with a deep stochastic phase modulation of partial components of the scattered field, the probability density functions of speckle intensity will tend to the same form corresponding to the case of the developed speckle field that is independent of the scattering system. The introduced parameters (the average speckle lifetime or the average frequency of threshold crossings) are determined by the characteristic time of reaching a certain critical value by the ensemble-averaged phase shift of interfering partial components of the scattered field regardless of the law of stochastic modulation of their phases. The critical value of the ensemble-averaged phase shift is determined only by an applied threshold level of speckle intensity.

At the same time, the decorrelation rate or the correlation time of intensity fluctuations are the *second-order* statistical characteristics that describe the ensemble-averaged or time-averaged relationship between intensity values at different times and are sensitive to the law of phase changes of partial components with time span.

Application of the discussed approach to the analysis of dynamic scattering of laser radiation in the evolving polylactide foams within the framework of the phenomenological model describing the relationship between the microscopic and macroscopic dynamics of expanding foam made it possible to reveal the fundamental features of formation of the foam structure depending on the foaming modes. In particular, the predicted linear relationship between the average speckle lifetime and the model parameter determined by the current foam volume and its first time derivative adequately describes the experimentally observed behavior of the system at low rates of pressure release, when the number of cells in the expanding foam remains constant or insignificantly varies. On the contrary, rapid depressurization causes appearance of new cells in the course of foam expansion. Accordingly, this causes a weaker dependence of the average speckle lifetime on the introduced model parameter.

Author Contributions: Conceptualization, D.Z.; methodology, D.Z.; software, M.A., E.U. and A.I.; validation, O.U., A.I. and E.I.; formal analysis, D.Z.; investigation, O.U., A.I. and E.I.; resources, D.Z.; data curation, M.A. and E.U.; writing—original draft preparation, D.Z., M.A. and E.U.; writing—review and editing, D.Z.; visualization, M.A., E.U. and A.I.; supervision, D.Z.; project administration, D.Z.; funding acquisition, D.Z. and A.I. All authors have read and agreed to the published version of the manuscript.

Funding: This work was supported by the Russian Foundation of Basic Research (project No. 18-29-06024). D.Z. acknowledges that the results of theoretical analysis were obtained within the framework of the State Assignment of the Institute for Problems of Precision Mechanics and Control, Russian Academy of Sciences (project No. 121022000123-8). A.I. acknowledges the support of this work in the part of the software development and speckle images processing by the Russian Science Foundation (project No. 21-79-00051).

Institutional Review Board Statement: Not applicable.

Informed Consent Statement: Not applicable.

Data Availability Statement: Not applicable.

Acknowledgments: The authors are grateful to A. Kh. Askarova for the literary editing of the manuscript.

Conflicts of Interest: The authors declare no conflict of interest.

References

1. Zhang, X. *Science and Principles of Biodegradable and Bioresorbable Medical Polymers. Materials and Properties*, 1st ed.; Woodhead Publishing: London, KY, USA, 2017; pp. 1–476.
2. Lanza, R.; Langer, R.; Vacanti, J. *Principles of Tissue Engineering*, 4th ed.; Academic Press: New York, NY, USA, 2013; pp. 83–123.
3. Kretlow, J.; Klouda, L.; Mikos, A. Injectable matrices and scaffolds for drug delivery in tissue engineering. *Adv. Drug Deliv. Rev.* **2007**, *59*, 263–273. [CrossRef]
4. Netti, P. (Ed.) *Biomedical Foams for Tissue Engineering Applications*, 1st ed.; Woodhead Publishing: London, KY, USA, 2014; pp. 1–446.
5. Salerno, A.; Oliviero, M.; Di Maio, E.; Iannace, S.; Netti, P. Design of porous polymeric scaffolds by gas foaming of heterogeneous blends. *J. Mater. Sci. Mater. Med.* **2009**, *20*, 2043–2051. [CrossRef]
6. White, L.J.; Hutter, V.; Tai, H.; Howdle, S.M.; Shakesheff, K.M. The effect of processing variables on morphological and mechanical properties of supercritical CO_2 foamed scaffolds for tissue engineering. *Acta Biomater.* **2012**, *8*, 61–71. [CrossRef]
7. Reverchon, E.; Cardea, S. Production of controlled polymeric foams by supercritical CO_2. *J. Supercrit. Fluids* **2007**, *40*, 144–152. [CrossRef]
8. Gualandi, G.; White, L.J.; Chen, L.; Gross, R.A.; Shakesheff, K.M.; Howdle, S.M.; Scandola, M. Scaffold for tissue engineering fabricated by non-isothermal supercritical carbon dioxide foaming of a highly crystalline polyester. *Acta Biomater.* **2010**, *6*, 130–136. [CrossRef] [PubMed]

9. Tai, H.; Mather, M.; Howard, D.; Wang, W.; White, L.; Crowe, J.; Morgan, S.P.; Chandra, A.; Williams, D.J.; Howdle, S.M.; et al. Control of pore size and structure of tissue engineering scaffolds produced by supercritical fluid processing. *Eur. Cells Mater.* **2007**, *14*, 64–77. [CrossRef]
10. Mathieu, L.M.; Montjovent, M.-O.; Bourban, P.-E.; Pioletti, D.P.; Månson, J.-A.E. Bioresorbable composites prepared by supercritical fluid foaming. *J. Biomed. Mater. Res. A* **2005**, *75*, 89–97. [CrossRef] [PubMed]
11. Karimi, M.; Heuchel, M.; Weigel, T.; Schossig, M.; Hoffmann, D.; Lendlein, A. Formation and size distribution of pores in poly(ε-caprolactone) foams prepared by pressure quenching using supercritical CO_2. *J. Supercrit. Fluids* **2012**, *61*, 175–190. [CrossRef]
12. Zimnyakov, D.; Alonova, M.; Ushakova, E.; Volchkov, S.; Ushakova, O.; Klimov, D.; Slavnetskov, I.; Kalacheva, A. Speckle-based sensing of microscopic dynamics in expanding polymer foams: Application of the stacked speckle history technique. *Sensors* **2021**, *21*, 6701. [CrossRef]
13. Zimnyakov, D.A.; Epifanov, E.O.; Kalacheva, A.V.; Minaev, N.V.; Minaeva, S.A.; Popov, V.K.; Samorodina, T.V.; Slavnetskov, I.O.; Ushakova, E.V.; Ushakova, O.V. Peculiarities of quasi-isothermal foaming of the SCF-plasticized polylactide: The effect of transition from foam expansion to its collapse. *Russ. J. Phys. Chem. B* **2020**, *14*, 1236–1243. [CrossRef]
14. Zimnyakov, D.A.; Popov, V.K.; Minaev, N.V.; Epifanov, E.O.; Parenago, O.O.; Zdrajevsky, R.A.; Vereshagin, D.A.; Ushakova, O.V. Competition of phase separation processes during quasi-isothermal foaming of polylactide in carbon dioxide environment. *Russ. J. Phys. Chem. B* **2020**, *14*, 1268–1276. [CrossRef]
15. Zimnyakov, D.; Zdrajevsky, R.; Minaev, N.; Epifanov, E.; Popov, V.; Ushakova, O. Extreme foaming modes for SCF-plasticized polylactides: Quasi-adiabatic and quasi-isothermal foam expansion. *Polymers* **2020**, *12*, 1055. [CrossRef] [PubMed]
16. Zimnyakov, D.A.; Bagratashvili, V.N.; Yuvchenko, S.A.; Slavnetskov, I.O.; Kalacheva, A.V.; Ushakova, O.V.; Markova, N.S. Quasi-adiabatic expansion of the polylactide foam: Features of the porous matrices formation in the region of transition between sub- and supercritical states of plasticizing carbon dioxide. *Russ. J. Phys. Chem. B* **2019**, *13*, 1254–1265. [CrossRef]
17. Thermophysical Properties of Fluid Systems. Available online: https://webbook.nist.gov/chemistry/fluid/ (accessed on 10 October 2021).
18. Pine, D.J.; Weitz, D.A.; Chaikin, P.M.; Herbolzheimer, E. Diffusing wave spectroscopy. *Phys. Rev. Lett.* **1988**, *66*, 1134–1136. [CrossRef]
19. Maret, G.; Wolf, P.E. Multiple light scattering from disordered media. The effect of Brownian motion of scatterers. *Z. Für Phys. B Condens. Matter* **1987**, *65*, 409–413. [CrossRef]
20. Weitz, D.A.; Zhu, J.X.; Durian, D.J.; Gang, H.; Pine, D.J. Diffusing-wave spectroscopy: The technique and some applications. *Phys. Scripta* **1993**, *T49*, 610–621. [CrossRef]
21. Menon, N.; Durian, D.J. Diffusing-wave spectroscopy of dynamics in a three-dimensional granular flow. *Science* **1997**, *275*, 1920–1922. [CrossRef]
22. Scheffold, F.; Romer, S.; Cardinaux, F.; Bissig, H.; Stradner, A.; Rojas-Ochoa, L.F.; Trappe, V.; Urban, C.; Skipetrov, S.E.; Cipelletti, L.; et al. New trends in optical microrheology of complex fluids and gels. In *Trends in Colloid and Interface Science XVI. Progress in Colloid and Polymer Science (Trends in Colloid and Interface Science XVI)*; Miguel, M., Burrows, H., Eds.; Springer: Berlin/Heidelberg, Germany, 2004; Volume 123, pp. 141–146.
23. Brunel, L.; Brun, A.; Snabre, P.; Cipelletti, L. Adaptive Speckle Imaging Interferometry: A new technique for the analysis of micro-structure dynamics, drying processes and coating formation. *Opt. Expr.* **2007**, *15*, 15250–15259. [CrossRef]
24. Viasnoff, V.; Lequeux, F. Multispeckle diffusing wave spectroscopy: A tool to study slow relaxation and time-dependent dynamics. *Rev. Sci. Instrum.* **2002**, *73*, 2336–2344. [CrossRef]
25. Snabre, P.; Crassous, J. Multispeckle diffusing wave spectroscopy of colloidal particles suspended in a random packing of glass spheres. *Eur. Phys. J. E* **2009**, *29*, 149–155. [CrossRef] [PubMed]
26. Weitz, D.; Pine, D. Diffusing-wave spectroscopy. In *Dynamic Light Scattering: The Method and Some Applications*; Brown, W., Ed.; Oxford University Press: Oxford, UK, 1993; pp. 652–720.
27. Ishimaru, A. Diffusion of light in turbid material. *Appl. Opt.* **1989**, *28*, 2210–2215. [CrossRef] [PubMed]
28. Prahl, S.A.; Keijzer, M.; Jacques, S.L.; Welch, A.J. A Monte Carlo model of light propagation in tissue. In *Dosimetry of Laser Radiation in Medicine and Biology*; Miller, G.J., Sliney, D.H., Eds.; SPIE Optical Engineering Press: Bellingham, WA, USA, 1989; pp. 102–111.
29. Goodman, J.W. Some fundamental properties of speckle. *J. Opt. Soc. Am.* **1976**, *66*, 1145–1150. [CrossRef]
30. Dainty, J.C. Some statistical properties of random speckle patterns in coherent and partially coherent illumination. *Opt. Acta* **1970**, *17*, 761–772. [CrossRef]
31. Vera, M.U.; Saint-Jalmes, A.; Durian, D.J. Scattering optics of foam. *Appl. Opt.* **2001**, *40*, 4210–4214. [CrossRef] [PubMed]